


Enhancement of Ablative Rayleigh-Taylor Instability Growth by Thermal Conduction Suppression in a Magnetic Field

Kazuki Matsuo^{1,*}, Takayoshi Sano^{1,†}, Hideo Nagatomo¹, Toshihiro Somekawa^{1,2}, King Fai Farley Law¹, Hiroki Morita¹, Yasunobu Arikawa¹, and Shinsuke Fujioka^{1,‡}

¹*Institute of Laser Engineering, Osaka University, Suita, Osaka 565-0871, Japan*

²*Institute for Laser Technology, 1-8-4 Utsubo-honmachi, Nishi-ku Osaka, Osaka 550-0004, Japan*

 (Received 15 June 2021; revised 6 September 2021; accepted 21 September 2021; published 12 October 2021)

Ablative Rayleigh-Taylor instability growth was investigated to elucidate the fundamental physics of thermal conduction suppression in a magnetic field. Experiments found that unstable modulation growth is faster in an external magnetic field. This result was reproduced by a magnetohydrodynamic simulation based on a Braginskii model of electron thermal transport. An external magnetic field reduces the electron thermal conduction across the magnetic field lines because the Larmor radius of the thermal electrons in the field is much shorter than the temperature scale length. Thermal conduction suppression leads to spatially nonuniform pressure and reduced thermal ablative stabilization, which in turn increases the growth of ablative Rayleigh-Taylor instability.

DOI: [10.1103/PhysRevLett.127.165001](https://doi.org/10.1103/PhysRevLett.127.165001)

Inertial confinement fusion (ICF) is created by imploding a spherical target to achieve high compression of the fuel and generate a high temperature hot spot to trigger ignition and maximize the thermonuclear energy gain. While progress towards the ICF ignition is being made at research facilities [1,2], the current central ignition scheme has not yet reached the ignition condition. Hot spark mixing with the cold dense fuel hampers fusion ignition mainly due to the significant growth of Rayleigh-Taylor (RT) instabilities [3–5] during the compression. Many current ICF research efforts are directed at understanding and controlling the growth of these asymmetries.

An alternate approach is to accept that perturbations are unavoidable in ICF experiments and instead reduce hot-spot cooling through the application of an external magnetic field. Perkins *et al.* [6] found that the application of a strong magnetic field to fusion targets relaxes the ignition requirements in two-dimensional (2D) magnetohydrodynamic (MHD) simulations. The nonuniformity of shape asymmetries increased with increasing field strength, giving an optimum applied field of around 50 T. Chang *et al.* [7] performed implosion experiments with seed magnetic field of 8 T, the symmetry change is not obvious with such a weak seed field. Walsh *et al.* [8–10] also found that the ignition requirements relaxed when hot-spot cooling was reduced in 3D extended-MHD simulations, however, RT growth increases in a magnetic field due to the reduced thermal ablative stabilization. The final hot spot shape is greatly distorted as a result of the growth of the RT instability enhanced by the magnetic field during the initial stage of implosion. While premagnetization of ICF implosions has the potential to enhance the fusion yield due to the

reduction of hot-spot cooling, enhancement of perturbation growth due to the magnetic field is unavoidable.

Although there have been several numerical studies on MHD phenomena in a high-energy density plasma (HEDP) [6,8–10], no experiments have been performed in this regime. Recently, it has become possible to generate high magnetic fields of more than 100 T in the laboratory, and it has become possible to investigate MHD phenomena in HEDPs, which were previously unexplored. A hydrodynamic instability experiment with the existence of the external magnetic field reported here is not only required for inertial confinement fusion research, but also provides a unique testbed for studying phenomena in astrophysics [11,12]. For example, Orland *et al.*, have performed numerical simulation of the interaction of a shock from a supernova remnant with a dense cloud with the magnetic field, and they found the disruption of the dense cloud due to the RT instability and other instabilities depends on the magnetic field geometry through the anisotropic thermal conduction [13].

The influence of the external magnetic field on the plasma manifests in two ways. First, the plasma motion is directly changed by the Lorentz force, though this effect is relatively small in our high- β plasma, where the parameter β is the ratio of the thermal and magnetic pressures:

$$\beta \approx 4.0 \left(\frac{B}{100 \text{ T}} \right)^{-2} \left(\frac{T_e}{100 \text{ eV}} \right) \left(\frac{n_e}{10^{21} \text{ cm}^{-3}} \right). \quad (1)$$

Hydrodynamic instability growth is reduced by the restitution force of the magnetic field bent by nonuniform plasma flow in a low- β plasma [14,15], whereas the thermal

pressure is always larger than the magnetic pressure in this study (i.e., $\beta \gg 1$).

Second, the electron energy increment is modified by the magnetic field through the thermal conductivity, where κ is the thermal conductivity tensor. Assuming 2D transport, κ is described as

$$\kappa \cdot \nabla T_e = \kappa_{\parallel} \nabla_{\parallel} T_e + \kappa_{\perp} \nabla_{\perp} T_e + \kappa_{\wedge} \nabla T_e, \quad (2)$$

$$\kappa_{\parallel} = \gamma_0 \left(\frac{n_e T_e \tau_e}{m_e} \right) = \gamma_0 \kappa_0, \quad (3)$$

$$\kappa_{\perp} = \kappa_0 \frac{\gamma'_1 \chi^2 + \gamma'_0}{\Delta}, \quad (4)$$

$$\kappa_{\wedge} = \kappa_0 \frac{\chi(\gamma''_1 \chi^2 + \gamma''_0)}{\Delta}, \quad (5)$$

where χ is the Hall parameter and $\Delta = \chi^4 + \delta_1 \chi^2 + \delta_0$. γ'_0 , γ'_1 , δ_1 , and δ_0 are the Braginskii coefficients [16], whose values vary with the magnetic field.

The Hall parameter is the product of the electron gyrofrequency (ω_c) and electron-ion collision time (τ_{ei}):

$$\omega_c \tau_{ei} \approx 1.3 \left(\frac{B}{100 \text{ T}} \right) \left(\frac{T_e}{100 \text{ eV}} \right)^{\frac{3}{2}} \left(\frac{n_e}{10^{21} \text{ cm}^{-3}} \right)^{-1}. \quad (6)$$

For a 300-eV polystyrene plasma, 200-T external magnetic field, and critical density for 351-nm laser beams, the Hall parameter is greater than unity. When the Hall parameter is nonzero, the external magnetic field reduces the electron thermal conduction across the magnetic field lines.

A basic experiment with a simple geometry was performed with a spatially uniform strong magnetic field generated by a pair of laser-driven capacitor coil targets. Three GEKKO-XII laser beams were used for each capacitor coil target to generate the magnetic field. The wavelength, pulse shape, pulse duration, and energy of the GEKKO-XII beams were 1.053 μm , Gaussian, 1.2 ns full width at half maximum, and 700 \pm 20 J per beam. The strength of the magnetic field generated with the capacitor-coil target was measured on the GEKKO-XII, LULI2000, Shengguang-II, and OMEGA-EP laser facilities [17–21]. 215 \pm 21 T magnetic fields were obtained in a previous experiment [22] with the same configuration.

Figure 1 shows the experimental layout and a face-on x-ray image and photograph of the target. A 16- μm -thick polystyrene (C_8H_8) foil was irradiated with laser beams midway between the two coils. The external magnetic field is in the same direction as the incoming laser beam. The width of the polystyrene foil was 400 μm . Initial sinusoidal perturbations for 30, 60, and 100- μm wavelengths (λ) with an initial amplitude 1.0 \pm 0.1 μm were imposed on the front side of the planar polystyrene foils. 15- μm tantalum plates were placed at the bottom and top of the

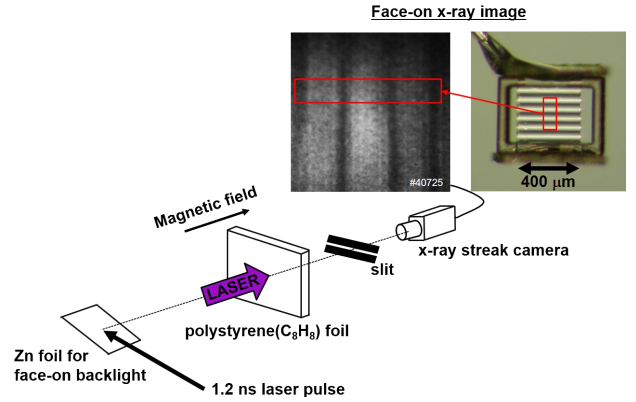


FIG. 1. Experimental setup. Face-on x-ray backlighting was used to measure the temporal evolution of the areal density modulations.

polystyrene foil to prevent the polystyrene foil from being preheated by x rays generated at the capacitor parts. Three 351-nm beams of the GEKKO-XII laser were used to drive the polystyrene foil at an intensity of $(2.5 \pm 0.1) \times 10^{14} \text{ W/cm}^2$.

The polystyrene foil with the pre-imposed perturbation is accelerated by the drive laser and is measured by backlighting x-rays emitted from a zinc foil that is irradiated by a separate laser. The laser-produced zinc plasmas emit relatively broad *L*-shell x rays centered at 1.5 keV [23]. 5.5- μm -thick Al (*K* absorption edge at 1.56 keV) and 25- μm -thick Be foils were placed in front of an x-ray streak camera (XSC) for x-ray filtering.

The intensity distribution of the x rays transmitted through the target is imaged on the XSC. The areal-density perturbation is thus recorded as the contrast of the x-ray intensity distribution, a technique known as “face-on x-ray backlighting” [23,24]. Face-on x-ray backlighting was used to measure the temporal evolution of the areal density modulations ($\Delta\rho a$) amplified by the hydrodynamic instability from the x-ray intensity ratio between the peaks (I_{peak}) and valleys (I_{valley}) of an image as $\Delta\rho a = \ln(I_{\text{peak}}/I_{\text{valley}})/2\mu$, where $\mu = 607 \text{ g/cm}^2$ is the mass absorption rate of polystyrene for the x rays. The spatial and temporal resolutions of the x-ray imaging system were measured to be 13 μm and 130 ps, respectively.

Figure 2 shows a face-on x-ray backlight image taken for a target with the modulation wavelength $\lambda = 60 \mu\text{m}$. We defined the time of 1 ns ($t = 1 \text{ ns}$) to be the drive laser peak time. Figures 2(a) and 2(b) show the cases without and with a magnetic field, respectively. Figures 2(c),2(d) show the profiles of the x-ray transmittance at $t = 1.25 \text{ ns}$ without a magnetic field and with a magnetic field, respectively. The black dots are the experimental results of x-ray transmittance evaluated from the line-out of the face-on x-ray backlight image. The red curves are the results of the two-dimensional magnetohydrodynamic code PINOCO-2D-MHD [25] with the Braginskii model of electron thermal

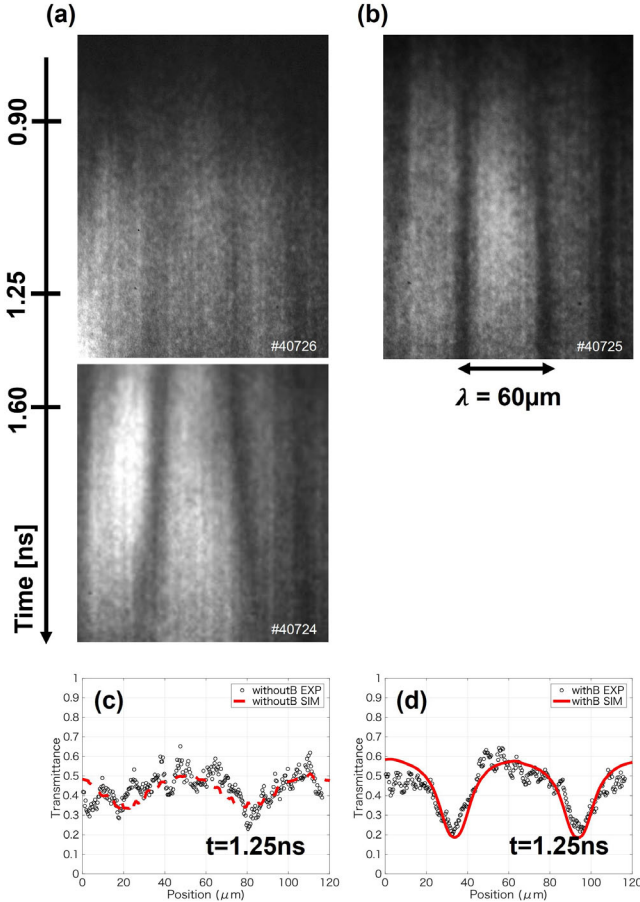


FIG. 2. Comparison of face-on x-ray radiographies of perturbation measured with an x-ray streak camera between the cases (a) without and (b) with the application of the external magnetic field. (c) and (d) Curve profiles at 1.25 ns of the radiographies corresponding to (a) and (b). Red solid curves in (c) and (d) are profiles calculated with PINOCO-2D-MHD simulation.

transport. The modulations grow faster in an external magnetic field than in the absence of a magnetic field.

Figure 3 shows the time evolution of the growth factors of the fundamental mode, where the growth factor is defined as the measured areal-density perturbation divided by the initial amplitude of $1.0 \pm 0.1 \mu\text{m}$. The black dots are the experimental results and the blue curves are the results of the MHD simulation. The simulation results exhibit a faster growth with a magnetic field than without a magnetic field.

Figure 4 shows the growth rate of the ablative RT instability. The plotted values are summarized in Table I. The growth rate of the RT instability is obtained from the exponential fit to the time history of the growth factor in a linear growth regime. We have defined the linear regime as that with an amplitude smaller than 10% of the wavelength. Similar results were also obtained in the other facilities for the case without a magnetic field [26,27]. Obviously, the growth rate in the external magnetic field are faster than that without a magnetic field.

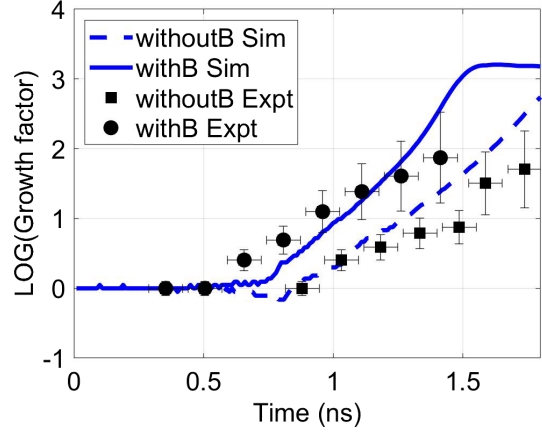


FIG. 3. Comparison of experimentally measured growth factors and calculated values with PINOCO-2D-MHD simulations for 60- μm wavelength perturbation with an initial amplitude of 1.0 μm . 2D hydrodynamic simulations show good agreement with experimental data. The experimental data are shown as circles and squares, and the calculated growth factors are shown as solid and dashed curves for the cases with and without external magnetic field.

The growth rate γ of the RT instability including the ablation effect was suggested by Bodner [28], and is approximated by the modified Takabe formula [29]:

$$\Gamma = \alpha \sqrt{\frac{kg}{1 + kL}} - \beta k V_a, \quad (7)$$

where α and β are coefficients, k is the wave number of the perturbation, g is gravity, L is the density scale length at the ablation surface, and V_a is the ablation velocity. In our experiment, $g = 75 \pm 5 \mu\text{m}/\text{ns}^2$ is calculated from a trace of the laser-driven polystyrene foil observed using an x-ray streak camera and side-on backlighting. The results of the PINOCO-2D-MHD simulation reproduce the velocity of

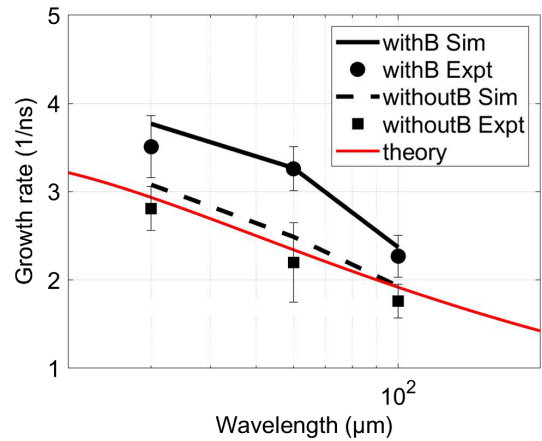


FIG. 4. Growth rate of the RT instability obtained from the exponential fit to the data of the growth factor in a linear growth regime.

TABLE I. Compilation of growth rates from experimental data and data from the PINOCO-2D-MHD simulation.

λ (μm)	Γ_{Expt} withoutB (ns^{-1})	Γ_{Sim} withoutB (ns^{-1})	Γ_{Expt} withB (ns^{-1})	Γ_{Sim} withB (ns^{-1})
30	2.81 ± 0.25	3.08	3.51 ± 0.35	3.77
60	2.20 ± 0.45	2.49	3.26 ± 0.25	3.27
100	1.76 ± 0.19	1.93	2.27 ± 0.24	2.37

the accelerated polystyrene foil. Near the laser peak time, $L \approx 1 \mu\text{m}$ and $V_a \approx 2 \mu\text{m}/\text{ns}$ are obtained from the simulation according to the procedure described in Ref. [30]. No significant changes in the ablation velocity and the acceleration of the foil due to the presence of the external magnetic field were found. Betti *et al.* found an analytical solution [30] for a plastic target, which corresponds to $\alpha = 0.98$ and $\beta = 1.7$ when approximated by Eq. (7). The theoretical growth rate is also shown in Fig. 4 by the red curve, which confirm the accuracy of the experimental measurements and the MHD simulations.

As a result of the perturbation growth, the peaks of the ablation-front ripple protrude into the hotter plasma corona, and the valleys recede toward the colder plasma corona. Since the temperature perturbation is flat in the laser absorption region, the temperature gradients and heat fluxes are enhanced at the peaks and reduced at the valleys, as shown in Fig. 5(a). An excess in the heat flux speeds up the ablation front, while a deficiency slows the front down, a process called ablative stabilization.

The hydrodynamic perturbation growth is affected by the external magnetic field as a result of the anisotropic thermal conductivity in the ablated plasma. The magnetic field lines move together with the ablated plasma due to its large magnetic Reynolds number. The direction of the ablated plasma flow is normal to the target surface, and ablated

plasma accumulates at the valleys of the sinusoidal perturbation. Therefore, the external magnetic field is compressed at the valleys and decompressed at the peaks of the sinusoidal perturbation, as shown in Fig. 5(b). The temperature increases at the valleys due to anisotropic thermal conduction in the perturbed magnetic field structure. The pressure distribution becomes spatially nonuniform. This nonuniformity affects the perturbation growth not only in the acceleration phase but also in the shock passage phase, which causes the early rise of the fluctuation in the magnetized case.

The ablative stabilization is also reduced by less thermal smoothing of the temperature perturbation in the compressed magnetic field. These lead to enhancement of the perturbation growth. We should note that the Nernst effect is neglected in this calculation mainly due to relatively high collisionality of the plasma [10].

When the magnetic field causes the timescale of the thermal diffusivity to be longer than the hydrodynamic timescale, heat is trapped inside the ablation plasma, affecting the fluid motion. The thermal diffusivity (η) is the thermal conductivity divided by the density and specific heat capacity at constant pressure. The timescale of the thermal diffusivity in the compressed magnetic field (η_{\perp}) is locally smaller than the hydrodynamic timescale on the wavelength scale (λ) of the perturbation. This leads to the following inequalities:

$$\frac{\lambda^2}{\eta} < \frac{\lambda}{C_s} < \frac{\lambda^2}{\eta_{\perp}}. \quad (8)$$

Solving these inequalities for the wavelength, we obtain the condition that the magnetic field can affect the ablative RT instability as

$$\frac{\eta}{C_s} \frac{1}{\sqrt{1 + (\omega_c \tau_{ei})^2}} < \lambda < \frac{\eta}{C_s}. \quad (9)$$

As shown in Fig. 5, the magnetic field is compressed and becomes inhomogeneous in the plasma corona, and the thermal conductivity is also quite anisotropic there. The corona plasma expands outward from the critical density where the incident laser is mainly absorbed. We used the plasma parameters at the critical density as indices of the corona plasma for calculating Eq. (9). For a 300-eV polystyrene plasma at critical density for 351-nm laser beams, $(\eta/C_s) \approx 120 \mu\text{m}$. In the compressed magnetic field, the Hall parameter is about $1 \sim 6$ at the critical density. Therefore, the growth rates of the ablative RT instability in our experiment with $\lambda = 30\text{--}100 \mu\text{m}$ are enhanced by the reduction of thermal transport due to the magnetic field (see Fig. 4).

In summary, RT instability growth experiments were performed to demonstrate unavoidable perturbation growth due to a magnetic field. The unstable modulation growth in

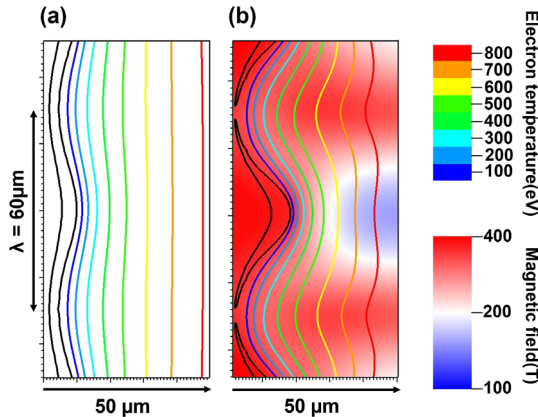


FIG. 5. Contours of electron temperature in a corona plasma produced from a corrugated CH foil whose wavelength is $60 \mu\text{m}$ (a) with and (b) without the application of external magnetic field. Magnetic field profile is overlaid on the contours in (b).

an external magnetic field was strongly increased compared to the growth in the absence of a field.

Previous numerical simulations with implosion geometries [6,9] have shown that the presence of a magnetic field can enhance the growth of hydrodynamic instabilities. Here, we have performed experiments and simulations with a planar geometry to reveal a relatively simple physical picture behind the complex phenomenon that combines magneto-hydrodynamics, radiation transport, and heat transport.

We also obtain the condition that the magnetic field can affect the ablative RT instability as Eq. (9). The stronger the magnetic field, the higher the modes of RT growth affected. In other words, by reducing the thermal transport at the instability growth front, the magnetization allows higher modes of RT instability to grow.

These effects must be considered in the design of magnetically assisted ICF, which may be an alternative to fusion ignition schemes. Srinivasan *et al.* [31] have pointed out that the strengths of the self-generated magnetic field and the Hall parameter in National Ignition Facility implosions are estimated to be of the order of $10^2 - 10^3$ T and in the range between 0.1 and 1, respectively. In such a strong self-generated magnetic field, anisotropic thermal conduction may affect hydrodynamic growth. The thermal conduction suppression due to a magnetic field at ignition-scale lasers requires further investigation.

The authors wish to thank the technical support staff of ILE and the Cyber Media Center at Osaka University for assistance with the laser operation, target fabrication, plasma diagnostics, and computer simulations. This research used the computational resources of the HPCI system provided by Information Technology Center, Nagoya University through the High Performance Computing Infrastructure (HPCI) System Research Project (Project ID: hp180093). This work was supported by the Collaboration Research Program between the National Institute for Fusion Science and the Institute of Laser Engineering at Osaka University, and by the Japanese Ministry of Education, Science, Sports, and Culture through Grants-in-Aid, KAKENHI (Grants No. 24684044, No. 25630419, No. 26287147, No. 15K17798, No. 15K21767, No. 15KK0163, No. 16K13918, No. 16H02245, and No. 17K05728), Bilateral Program for Supporting International Joint Research by JSPS, Grants-in-Aid for Fellows by Japan Society for The Promotion of Science (Grants No. 14J06592, No. 15J00850, No. 15J00902, No. 15J02622, No. 17J07212, No. 18J01627, No. 18J11119, and No. 18J11354), Matsuo Research Foundation, and the Research Foundation for Opto-Science and Technology.

* matsuo-k@ile.osaka-u.ac.jp

† sano@ile.osaka-u.ac.jp

‡ sfujioka@ile.osaka-u.ac.jp

- [1] S. Le Pape *et al.*, *Phys. Rev. Lett.* **120**, 245003 (2018).
- [2] S. P. Regan *et al.*, *Phys. Rev. Lett.* **117**, 025001 (2016).
- [3] Y. Zhou, *Phys. Rep.* **720–722**, 1 (2017).
- [4] Y. Zhou, *Phys. Rep.* **723–725**, 1 (2017).
- [5] B. A. Remington, R. P. Drake, and D. D. Ryutov, *Rev. Mod. Phys.* **78**, 755 (2006).
- [6] L. J. Perkins, D. D.-M Ho, B. G. Logan, G. B. Zimmerman, M. A. Rhodes, D. J. Strozzi, D. T. Blackfield, and S. A. Hawkins, *Phys. Plasmas* **24**, 062708 (2017).
- [7] P. Y. Chang, G. Fiksel, M. Hohenberger, J. P. Knauer, R. Betti, F. J. Marshall, D. D. Meyerhofer, F. H. Séguin, and R. D. Petrasso, *Phys. Rev. Lett.* **107**, 035006 (2011).
- [8] C. A. Walsh, K. McGlinchey, J. K. Tong, B. D. Appelbe, A. Crilly, M. F. Zhang, and J. P. Chittenden, *Phys. Plasmas* **26**, 022701 (2019).
- [9] C. A. Walsh, A. Crilly, and J. Chittenden, *Nucl. Fusion* **60**, 106006 (2020).
- [10] C. A. Walsh, J. P. Chittenden, D. W. Hill, and C. Ridgers, *Phys. Plasmas* **27**, 022103 (2020).
- [11] H. Isobe, T. Miyagoshi, K. Shibata, and T. Yokoyama, *Nature (London)* **434**, 478 (2005).
- [12] D. Lecoanet, I. J. Parrish, and E. Quataert, *Mon. Not. R. Astron. Soc.* **423**, 1866 (2012).
- [13] S. Orlando, F. Bocchino, F. Reale, G. Peres, and P. Pagano, *Astrophys. J.* **678**, 274 (2008).
- [14] J. M. Stone and T. Gardiner, *Phys. Fluids* **19**, 094104 (2007).
- [15] T. Sano, T. Inoue, and K. Nishihara, *Phys. Rev. Lett.* **111**, 205001 (2013).
- [16] S. I. Braginskii, *Rev. Plasma Phys.* **1**, 205 (1965), <https://ui.adsabs.harvard.edu/abs/1965RvPP...1..205B/abstract>.
- [17] K. F. F. Law *et al.*, *Appl. Phys. Lett.* **108**, 091104 (2016).
- [18] S. Fujioka *et al.*, *Sci. Rep.* **3**, 1170 (2013).
- [19] B. J. Zhu *et al.*, *Appl. Phys. Lett.* **107**, 261903 (2015).
- [20] J. J. Santos *et al.*, *New J. Phys.* **17**, 083051 (2015).
- [21] L. Gao, H. Ji, G. Fiksel, W. Fox, M. Evans, and N. Alfonso, *Phys. Plasmas* **23**, 043106 (2016).
- [22] K. Matsuo *et al.*, *Phys. Rev. E* **95**, 053204 (2017).
- [23] H. Azechi, T. Sakaiya, S. Fujioka, Y. Tamari, K. Otani, K. Shigemori, M. Nakai, H. Shiraga, N. Miyanaga, and K. Mima, *Phys. Rev. Lett.* **98**, 045002 (2007).
- [24] T. Sakaiya, H. Azechi, M. Matsuoka, N. Izumi, M. Nakai, K. Shigemori, H. Shiraga, A. Sunahara, H. Takabe, and T. Yamanaka, *Phys. Rev. Lett.* **88**, 145003 (2002).
- [25] H. Nagatomo, T. Johzaki, A. Sunahara, H. Sakagami, K. Mima, H. Shiraga, and H. Azechi, *Nucl. Fusion* **53**, 063018 (2013).
- [26] S. G. Glendinning *et al.*, *Phys. Rev. Lett.* **78**, 3318 (1997).
- [27] V. A. Smalyuk, S. X. Hu, V. N. Goncharov, D. D. Meyerhofer, T. C. Sangster, C. Stoeckl, and B. Yaakobi, *Phys. Plasmas* **15**, 082703 (2008).
- [28] S. E. Bodner, *Phys. Rev. Lett.* **33**, 761 (1974).
- [29] H. Takabe, L. Montierth, and R. L. Morse, *Phys. Fluids* **26**, 2299 (1983).
- [30] R. Betti, V. N. Goncharov, R. L. McCrory, and C. P. Verdon, *Phys. Plasmas* **5**, 1446 (1998).
- [31] B. Srinivasan and X. Z. Tang, *Phys. Plasmas* **19**, 082703 (2012).